Struct Multidisc Optim (2009) 39:327–336
DOI 10.1007/s00158-008-0342-4

BIOMECHANICAL APPLICATION

Size optimization of a cantilever beam under deformation-dependent loads with application to wheat stalks

P. Sivanagendra · G. K. Ananthasuresh

Received: 8 January 2008 / Revised: 27 September 2008 / Accepted: 9 November 2008 / Published online: 14 January 2009

Abstract In this paper, we consider the optimization of the cross-section profile of a cantilever beam under deformation-dependent loads. Such loads are encountered in plants and trees, cereal crop plants such as wheat and corn in particular. The wind loads acting on the grain-bearing spike of a wheat stalk vary with the orientation of the spike as the stalk bends; this bending and the ensuing change in orientation depend on the deformation of the plant under the same load. The uprooting of the wheat stalks under wind loads is an unresolved problem in genetically modified dwarf wheat stalks. Although it was thought that the dwarf varieties would acquire increased resistance to uprooting, it was found that the dwarf wheat plants selectively decreased the Young's modulus in order to be compliant. The motivation of this study is to investigate why wheat plants prefer compliant stems. We analyze this by seeking an optimal shape of the wheat plant's stem, which is modeled as a cantilever beam, by taking the large deflection of the stem into account with the help of co-rotational finite element beam modeling. The criteria considered here include minimum moment at the fixed ground support, adequate stiffness and strength, and the volume of material. The result reported here is an example of flexibility, rather than stiffness, leading to increased strength.

Keywords Deformation-dependent loads · Size optimization · Dwarf wheat stalks · Compliant design

List of symbols

E	Young's modulus of material
F	Aerodynamic load
C_{D}	Drag coefficient
C_{L}	Lift coefficient
F_{D}	Drag force
F_{L}	Lift force
ρ	Mass density
A	Area of cross-section of the beam
A_{f}	Frontal area
V	Air-flow velocity
ϕ	Angle of the rotated spike with the vertical
α	Rigid body rotation of the beam element
$\mathbf{P}_{\mathrm{g}}$	Degrees of freedom in the global coordinate system
$\mathbf{P}_{\mathrm{l}}$	Degrees of freedom in the local coordinate system
$\mathbf{f}_{\mathrm{int}}$	Internal force vector
$\mathbf{f}_{\mathrm{ext}}$	External force vector
$\mathbf{K}_{t\_\mathrm{int}}$	Global tangent stiffness matrix due to internal forces
$\mathbf{K}_{t\_\mathrm{ext}}$	Global tangent stiffness matrix due to external forces
$\mathbf{U}_0$	Global reference displacement vector
$\Delta\mathbf{U}$	Global incremental displacement vector
ε	Strain in the beam element

This work was presented at the 7th World Congress on Structural and Multidisciplinary Optimization (WCSMO-7), May 21–25, 2007, Seoul, Korea.

P. Sivanagendra · G. K. Ananthasuresh (✉)
Mechanical Engineering Department,
Indian Institute of Science,
Bangalore 560012, India
e-mail: suresh@mecheng.iisc.ernet.in

P. Sivanagendra
e-mail: psivanagendra@gmail.com

σ	Stress in the beam element
M_{R}	Ground reaction moment
d_{l}	Lower bound on the diameter of the stem
d_{u}	Upper bound on the diameter of the stem
$d(x)$	Diameter of the stem along its axis
S	Permissible stress
Δ	Permissible lateral deflection
L	Length
L_0	Initial length
u	Nodal axial deflection in the global coordinate system
w	Nodal transverse deflection in the global coordinate system
θ	Nodal rotation of the element in the global coordinate system
$\overline{u}$	Nodal axial deflection in the local coordinate system
$\overline{\theta}$	Nodal rotation in the local coordinate system
V^*	Permissible volume of the stem

1 Introduction

Wind-related crop damage is a major obstacle to cereal production (mainly in wheat) that costs several billion dollars per year (Farquhar et al. 2002). Mechanical damage to the wheat plant is due to wind-induced stress (Norman 1986), resonance (Miller 2005), anchorage rotation, and buckling under its own weight (Farquhar et al. 2002). These biomechanical factors play an important role in the growth and endurance of wheat plants. Hence, the plant biomechanics continues to be an important area of study. The "reduced height" Rht genes, known as the *dwarfing genes*, have been used to make the plants grow short with a view to mitigate the aforementioned problems and thereby increase the yield (Borojevic 2005). A study that measured the elastic moduli of the dwarf variety of wheat plants found that dwarf plants reduced their effective moduli selectively (Farquhar and Meyer-Phillips 2001; Farquhar et al. 2004). This can be interpreted as the plant's preference to be compliant (i.e., elastically flexible) even when they are forcibly made to grow shorter than their normal height through genetic modification. By means of a simple optimization problem, we argue in this paper that compliance is indeed preferred under some assumed performance criteria for wheat plants.

While stress, resonance, and buckling are familiar terms to engineers, "anchorage rotation" is a new term. It refers to one of the main modes of failure wherein the plant is uprooted at the ground anchor. Agricultural scientists call this failure *dislodging*. If we model the vertically growing plant's stem as a cantilever beam, then the anchorage rotation is a consequence of the reaction moment at the ground anchor. Minimizing this moment helps prevent anchorage rotation. Adequate strength and stiffness are also additional criteria while the mass of the material of the stem is limited. The mass of the material for the plant stem is a limited resource because there is competition between the growing spike with grains and the rest of the plant. Thus, optimization is inherent in plants' stems to satisfy all these criteria.

From the viewpoint of structural optimization, the optimization of the plant stem of wheat is an interesting problem in two ways. First, the wind loads acting on the plant stems are deformation-dependent. This is because significant wind loads act primarily on the grain/flower bearing spike at the tip. This load changes as the orientation of the spike changes due to the deformation caused by the wind load itself (see Fig. 1). So, the load here is dependent on the deformation—a situation that is considered in fluid-structure interaction problems involving large displacements (Moller 2002).

The second interesting aspect of this problem is that there is a conflict between compliant and stiff designs in plant stems. If we consider that the aerodynamic load on the spike can be given by the following formula (Hoerner 1965), we can see that the increased deformation helps reduce the tip load, which can be approximated as

$$F = \frac{1}{2} C_{\mathrm{D}} \rho A_{\mathrm{f}} V^2 = F_0 \cos\phi \tag{1}$$

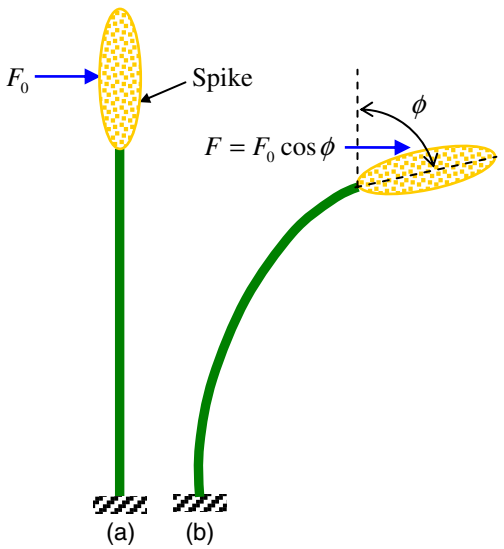

Fig. 1 Deformation-dependent loads on plant stems: **a** undeformed state, **b** deformed state

where F is the aerodynamic load on an elliptically shaped object oriented at an angle ϕ with the direction perpendicular to that of the air-flow velocity, V. Here, the drag coefficient C_D, frontal area A_f, mass density ρ, and V are combined into a constant term F_0. The $\cos\phi$ term includes the effect of the orientation. When the plant deforms and bends more, not only the tip load reduces but also the moment arm relative to the ground anchor reduces. Consequently, the reaction moment at the ground anchor reduces. Thus, there are two motivations for preferring compliant (i.e., flexible) stems. But excessive deformation due to large flexibility has other problems. These are: breaking of the stem due to excessive stress; excessive deformation that makes the plant interfere with its neighbors; resonant behavior under varying wind loads; and finally buckling under the self-weight. Thus, plants seem to seek an optimal configuration for adequate stiffness, strength against buckling and material failure, and resonance while preventing anchorage rotation due to the reaction moment felt at the ground anchor. There is also the limited resource condition of available mass as the plant grows and sustains itself.

In order to investigate whether plants prefer compliant or stiff stems in the aforementioned conflicting requirements, in this paper we consider the size-optimization of a plant's stem by modeling it as a cantilever beam. We include the large deformation effects. As noted above, the load depends on the deformation which is taken into account in the geometrically nonlinear finite element analysis with co-rotational beam elements (Crisfield 1991). Due to this kind of loading pattern, there will be an additional contribution to the tangent stiffness matrix due to the external load (Sivanagendra 2006). For simplicity and the lack of information, we consider only linearly elastic material behavior. The properties of wheat plants' stems are taken from Farquhar et al. (2002). In addition to the load on the spike, there exists distributed load all along the stem and leaves but it is considered to be negligible when compared with the load on the spike.

The problem is posed in different ways so that we understand the criteria that resolve the conflict between compliant and stiff designs for the plant's stem. Prevention of the anchorage rotation is taken as the primary criterion. Stiffness and strength are taken as secondary criteria. Buckling and resonance are not considered in this paper although they are important in the overall behavior of the plant in its operating environment.

The remainder of the paper is organized as follows. In the next section, we include the details of how we dealt with the large-displacement analysis of the beam under the deformation-dependent loading. Following this, we present different formulations of the optimization problem and the results. Discussion and concluding remarks are in the last section of the paper.

2 Large displacement analysis with deformation-dependent loading

We use large-displacement co-rotational finite element formulation (Crisfield 1991) for the analysis of 2D beams using two-noded elements. We consider a beam element undergoing large displacement and rotation as shown in Fig. 2. Let $\mathbf{P}_g = \{u_1\ w_1\ \theta_1\ u_2\ w_2\ \theta_2\}^T$ be the column vector that denotes the displacements in the X and Y directions and rotation about the Z axis at the first and second nodes in the chosen global coordinate system, XYZ. In the co-rotational formulation, we need to subtract the rigid body rotation α of the element. After we do that, the local degrees of freedom of the beam element are expressed as $\mathbf{P}_l = \{\bar{u}\ \bar{\theta}_1\ \bar{\theta}_2\}^T$ where

$$\begin{aligned} \bar{u} &= \text{change in the length of the beam} = L - L_0 \\ \bar{\theta}_1 &= \theta_1 - \alpha \\ \bar{\theta}_2 &= \theta_2 - \alpha \end{aligned} \tag{2}$$

where the expressions for L_0, L and α are obtained using the global coordinates $\{x_1, z_1, x_2, z_2\}$ of the beam element and its global degrees of freedom, $\mathbf{P}_g = \{u_1\ w_1\ \theta_1\ u_2\ w_2\ \theta_2\}^T$. By using the following shape functions to interpolate the axial and transverse displacements with the local nodal variables of (2), we can write the displacement u_1 at any point with coordinates

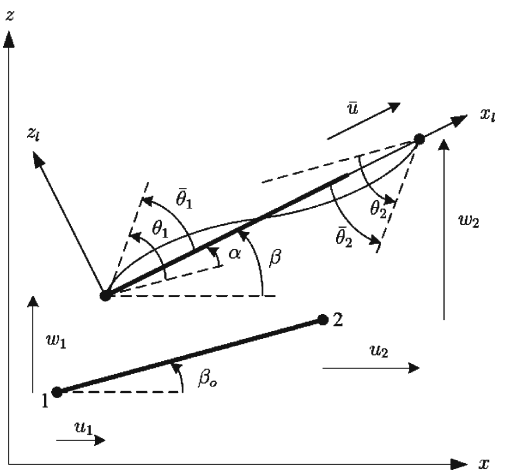

Fig. 2 Beam kinematics in co-rotational formulation

x and z in the axial and transverse directions respectively in the local coordinate system, xyz.

$$
\begin{aligned}
u_{\mathrm{na}} &= \frac{x}{L_0}\overline{u} = \zeta\overline{u} \\
w_{\mathrm{l}} &= L_0\left\{\zeta\,(1-\zeta)^2\,\overline{\theta}_1 + \zeta^2\,(1-\zeta)\,\overline{\theta}_2\right\} \\
u_{\mathrm{l}} &= u_{\mathrm{na}} - z\frac{dw_{\mathrm{l}}}{dx}
\end{aligned}
\tag{3}
$$

We use a shallow arch based modified strain measure that avoids membrane locking (Battini 2002), which is shown below.

$$
\varepsilon = \frac{1}{L}\int_0^L \left\{\frac{\partial u_{\mathrm{l}}}{\partial x} + \frac{1}{2}\left(\frac{\partial w_{\mathrm{l}}}{\partial x}\right)^2\right\} dx - z\frac{\partial^2 w_{\mathrm{l}}}{\partial x^2} \tag{4}
$$

The local and then the global tangent stiffness matrices are derived using the general method described in Crisfield (1991). By using the strain measure of (4), we present the essential details of the derivation given in Sivanagendra (2006) as described below.

By substituting for the interpolated displacements from (3) into (4), we write the strain as follows.

$$
\begin{aligned}
\varepsilon = {} & \frac{\overline{u}}{L_o} + \frac{1}{15}\left(\overline{\theta}_1^2 - \frac{\overline{\theta}_1\overline{\theta}_2}{2} + \overline{\theta}_2^2\right) \\
& + \frac{z}{L}\left((4-6\zeta)\,\overline{\theta}_1 + (2-6\zeta)\,\overline{\theta}_2\right)
\end{aligned}
\tag{5}
$$

We assume that the material is linearly elastic and write the stress as shown below.

$$
\sigma = E\varepsilon \tag{6}
$$

where E is the Young's modulus of the material.

The internal virtual work, IVW, in the beam element can be written by using the stress and strain from (6) and (5).

$$
IVW = \int_V \sigma\ \delta\varepsilon\ dV \tag{7}
$$

By defining the reaction forces and moments in the local coordinate system, $\mathbf{F}_{\mathrm{l}} = \{N,\ M_1,\ M_2\}$, we can write an alternate expression for IVW.

$$
IVW = \mathbf{F}_{\mathrm{l}}^{\mathrm{T}}\delta\mathbf{P}_{\mathrm{l}} = \left\{N\ M_1\ M_2\right\}^{\mathrm{T}}\delta\mathbf{P}_{\mathrm{l}} \tag{8}
$$

By equating (7) and (8), we can obtain the expressions for the internal reactions as follows.

$$
N = EA\left\{\frac{\overline{u}}{L_0} + \frac{1}{15}\left(\overline{\theta}_1^2 - \frac{\overline{\theta}_1\overline{\theta}_2}{2} + \overline{\theta}_2^2\right)\right\} \tag{9a}
$$

$$
\begin{aligned}
M_1 = {} & EAL_0\left\{\frac{\overline{u}}{L_0} + \frac{1}{2}\left(\overline{\theta}_1^2 - \frac{\overline{\theta}_1\overline{\theta}_2}{2} + \overline{\theta}_2^2\right)\right\} \\
& \times\left(\frac{2}{15}\overline{\theta}_1 - \frac{1}{30}\overline{\theta}_2\right) + \frac{EI}{L_0}\left(4\overline{\theta}_1 + 2\overline{\theta}_2\right)
\end{aligned}
\tag{9b}
$$

$$
\begin{aligned}
M_2 = {} & EAL_0\left\{\frac{\overline{u}}{L_0} + \frac{1}{15}\left(\overline{\theta}_1^2 - \frac{\overline{\theta}_1\overline{\theta}_2}{2} + \overline{\theta}_2^2\right)\right\} \\
& \times\left(\frac{2}{15}\overline{\theta}_1 - \frac{1}{30}\overline{\theta}_2\right) + \frac{EI}{L_0}\left(2\overline{\theta}_1 + 4\overline{\theta}_2\right)
\end{aligned}
\tag{9c}
$$

where I is the moment of inertia of the beam element that arises in the volume integration in (7). In order to compute the internal force vector in the global coordinate system, we use the following equality between internal work expressions computed in the local and global coordinate systems.

$$
\delta\mathbf{P}_{\mathrm{l}}^{\mathrm{T}}\mathbf{F}_{\mathrm{l}} = \delta\mathbf{P}_{\mathrm{g}}^{\mathrm{T}}\mathbf{F}_{\mathrm{g}} \tag{10}
$$

By referring to Fig. 2 and differentiating (2), we can obtain the transformation Jacobian between the local and global displacements.

$$
\delta\mathbf{P}_{\mathrm{l}} = \mathbf{B}\delta\mathbf{P}_{\mathrm{g}} \tag{11}
$$

with

$$
\mathbf{B} = \begin{bmatrix} -c & -s & 0 & c & s & 0 \\ -s/L & c/L & 1 & s/L & -c/L & 0 \\ -s/L & c/L & 0 & s/L & -c/L & 1 \end{bmatrix} \tag{12a}
$$

and

$$
\begin{aligned}
L &= \sqrt{(x_2 + u_2 - x_1 - u_1)^2 + (z_2 + w_2 - z_1 - w_1)^2} \\
c &= \frac{x_2 + u_2 - x_1 - u_1}{L} \\
s &= \frac{z_2 + w_2 - z_1 - w_1}{L}
\end{aligned}
\tag{12b}
$$

From (10) and (11), we can write $\mathbf{F}_{\mathrm{g}}$ as follows.

$$
\mathbf{F}_{\mathrm{g}} = \mathbf{B}^{\mathrm{T}}\mathbf{F}_{\mathrm{l}} \tag{13}
$$

In order to obtain the tangent stiffness matrix in the global coordinate system, we take the first variation of $\mathbf{F}_{\mathrm{g}}$ with respect to the global displacement vector.

$$
\delta\mathbf{F}_{\mathrm{g}} = \mathbf{K}_{\mathrm{g}}\delta\mathbf{P}_{\mathrm{g}} = \mathbf{B}^{\mathrm{T}}\delta\mathbf{F}_{\mathrm{l}} + N\delta\mathbf{b}_1 + M_1\delta\mathbf{b}_2 + M_2\delta\mathbf{b}_3 \tag{14}
$$

where $\mathbf{b}_i$ $(i = 1, 2, 3)$ are the columns of $\mathbf{B}$. The first of as yet unknown terms on the right hand side of (14) can be obtained as follows.

$$
\delta\mathbf{F}_{\mathrm{l}} = \mathbf{K}_{\mathrm{l}}\delta\mathbf{P}_{\mathrm{l}} = \mathbf{K}_{\mathrm{l}}\mathbf{B}\delta\mathbf{P}_{\mathrm{g}} \tag{15}
$$

where $\mathbf{K}_\mathrm{l}$ can be obtained by writing the internal strain energy using (5) and (6) and taking its derivative with respect to the local displacement vector, which yields:

$$\mathbf{K}_\mathrm{l} = \begin{bmatrix} K_\mathrm{l}^{11} & K_\mathrm{l}^{12} & K_\mathrm{l}^{13} \\ Sym & K_\mathrm{l}^{22} & K_\mathrm{l}^{23} \\ Sym & Sym & K_\mathrm{l}^{33} \end{bmatrix} \tag{16}$$

where

$$K_\mathrm{l}^{11} = \frac{EA}{L_0} \tag{17a}$$

$$K_\mathrm{l}^{12} = EA\left(\frac{2\bar{\theta}_1}{15} - \frac{\bar{\theta}_2}{30}\right) \tag{17b}$$

$$K_\mathrm{l}^{13} = EA\left(\frac{2\bar{\theta}_2}{15} - \frac{\bar{\theta}_1}{30}\right) \tag{17c}$$

$$K_\mathrm{l}^{22} = EAL_0\left(\frac{2\bar{\theta}_1}{15} - \frac{2\bar{\theta}_2}{30}\right) + \frac{2}{15}EAL_0\left(\frac{\bar{u}}{L_0} + \frac{\bar{\theta}_1^2}{15} - \frac{\bar{\theta}_1\bar{\theta}_2}{30} + \frac{\bar{\theta}_2^2}{15}\right) + \frac{4EI}{L_0} \tag{17d}$$

$$K_\mathrm{l}^{23} = EAL_0\left(\frac{2\bar{\theta}_2}{15} - \frac{\bar{\theta}_1}{30}\right)\left(\frac{2\bar{\theta}_1}{15} - \frac{\bar{\theta}_2}{30}\right) - \frac{1}{30}EAL_0\left(\frac{\bar{u}}{L_0} + \frac{\bar{\theta}_1^2}{15} - \frac{\bar{\theta}_1\bar{\theta}_2}{30} + \frac{\bar{\theta}_2^2}{15}\right) + \frac{2EI}{L_0} \tag{17e}$$

$$K_\mathrm{l}^{33} = EAL_0\left(\frac{2\bar{\theta}_2}{15} - \frac{\bar{\theta}_1}{30}\right)^2 + \frac{2}{15}EAL_0\left(\frac{\bar{u}}{L_0} + \frac{\bar{\theta}_1^2}{15} - \frac{\bar{\theta}_1\bar{\theta}_2}{30} + \frac{\bar{\theta}_2^2}{15}\right) + \frac{4EI}{L_0} \tag{17f}$$

where A is the area of cross-section of the beam element. The second to fourth unknown terms on the right hand side of (14) are obtained by differentiating the columns of A with respect to the displacements using (12a) and (12b). Thus, we can compute the element level tangent stiffness matrix in the global stiffness matrix from (14) and then the complete matrix for the entire structure by assembling all the elemental matrices into a global one.

The tangent stiffness matrix derived above is needed when the static equilibrium equation is linearized for solving it using the incremental-iterative method. The difference between the normal procedure and that of the deformation-dependent external load can be seen below.

$$\mathbf{f}_\mathrm{int} = \mathbf{f}_\mathrm{ext} \tag{18a}$$

$$\mathbf{f}_\mathrm{int}(\mathbf{U}_0) + \mathbf{K}_{t\_\mathrm{int}}\Delta\mathbf{U} = \mathbf{f}_\mathrm{ext}(\mathbf{U}_0) + \mathbf{K}_{t\_\mathrm{ext}}\Delta\mathbf{U} \tag{18b}$$

where $\mathbf{f}_\mathrm{int}$ is the internal force, $\mathbf{f}_\mathrm{ext}$ the external force, $\mathbf{K}_{t\_\mathrm{int}}$ and $\mathbf{K}_{t\_\mathrm{ext}}$ the tangent stiffness matrices of the internal and external forces respectively, $\mathbf{U}_0$ a reference displacement, and $\Delta\mathbf{U}$ the incremental/iterative displacement change. The re-arrangement of (18b) yields:

$$\Delta\mathbf{U} = \left[\mathbf{K}_{t\_\mathrm{int}} - \mathbf{K}_{t\_\mathrm{ext}}\right]^{-1}\{\mathbf{f}_\mathrm{ext}(\mathbf{U}_0) - \mathbf{f}_\mathrm{int}(\mathbf{U}_0)\} \tag{19}$$

This equation is used to iteratively compute the change in the displacements until convergence.

The external force for a two-noded beam element, which is modeled as a slender cylinder, due to drag and lift forces is shown in Fig. 3 and (20b) below. An approximate version of this was given in (1).

$$\mathbf{f}_{\mathrm{e\_ext}} = \{0\ 0\ 0\ F_\mathrm{D}\ F_\mathrm{L}\ 0\}^\mathrm{T} \tag{20a}$$

where

$$F_\mathrm{L} = \frac{1}{2}C_\mathrm{L}\rho A_f V^2 \text{ and } F_\mathrm{D} = \frac{1}{2}C_\mathrm{D}\rho A_f V^2 \tag{20b}$$

$$C_\mathrm{D} = 1.1\cos^3\phi + 0.02$$

$$C_\mathrm{L} = 1.1\cos^3\phi\sin\phi \tag{20c}$$

where ϕ is as shown in Fig. 3, ρ is the mass density, and V is the speed of the wind. The tangent stiffness matrix of the external force on an element can be obtained by taking the derivative of the force with respect to the nodal displacement vector $\mathbf{U}_\mathrm{e}$. Because the wind load acts on only the last finite element and that too on the far-end node, the 6×6 matrix $\mathbf{K}_{\mathrm{e\_ext}}$ is computed by differentiating (20a) with respect to the displacement vector of the tip element. For this, we note that angle ϕ is equal to the rigid-body rotation of the tip element, α, shown in Fig. 2. Since α, as can be seen in Fig. 2,

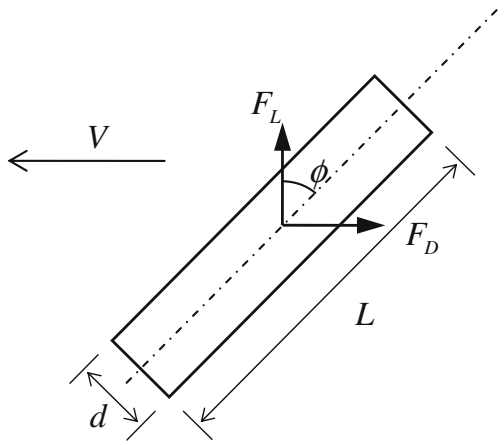

Fig. 3 Drag and lift forces on a cylinder subjected to steady wind

depends on the x and z displacements of the two nodes of the element (i.e., u_1, w_1, u_2, and w_2), only those elements of $\mathbf{K}_{e\_ext}$ that correspond to u_1, w_1, u_2, and w_2 are non-zero.

To validate the numerical solution technique of the deformation-dependent load, we bench-marked it against the commercial finite element solver, ABAQUS (www.simulia.com). Deformation-dependent load is of two types:

(a) the first is the "follower load" problem where only the direction of the load changes with the orientation of the element on which the load is acting. A classic example of this is a cantilever beam with a tip load that is always normal to the beam as the beam bends.
(b) the second is a situation where the magnitude of the load depends on the deformation.

Here, we have a general situation where both the direction and magnitude are changing. Most commercial finite element software can deal with only the first type, i.e., the follower load case. Hence, we solve this problem in order to benchmark our analysis results. In Fig. 4, we can see the good agreement between the results of ABAQUS and our implementation (labeled FEM in the figure) for the follower load case.

In lieu of verification of the general deformation-dependent load case using another software, we conducted an experiment in a wind tunnel (see Figs. 5 and 6). A cylindrical piece of foam was used to model the grain-bearing spike of the wheat plant and a steel wire was used to model the stem. The wire was mounted like a cantilever beam by fixing it to a stand. A pitot static tube was placed to measure the wind speed. The displacement of the wire (70 mm long and 2 mm in diameter) and the foam-cylinder (20 mm diameter and 25 mm tall) were measured using image processing of the photograph captured using a digital camera. The image of the deflected wire is shown in Fig. 6 and the comparison between simulation and the experiment is shown in Table 1. The relative error is less than 10% barring one case of 18% relative error for a quantity which is very low. We attribute the errors to the measurement error in capturing the displacements and possibly due to misalignments in mounting the wire inside the wind tunnel. This simple experiment confirms that the numerical modeling of the deformation-dependent loading is reasonably accurate.

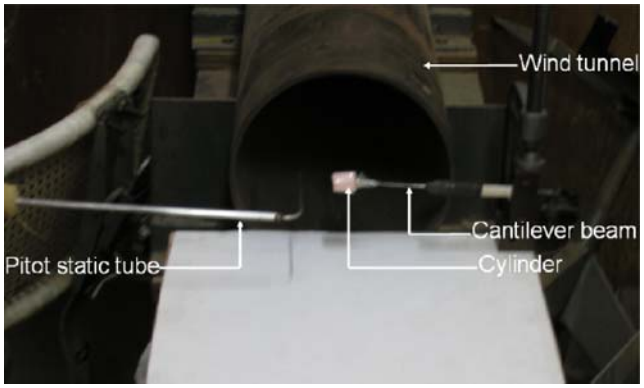

Fig. 5 Experimental setup to induce deformation-dependent loads on a cantilever beam as a model of a wheat plant with a grain-bearing spike subjected to wind loads in a wind tunnel

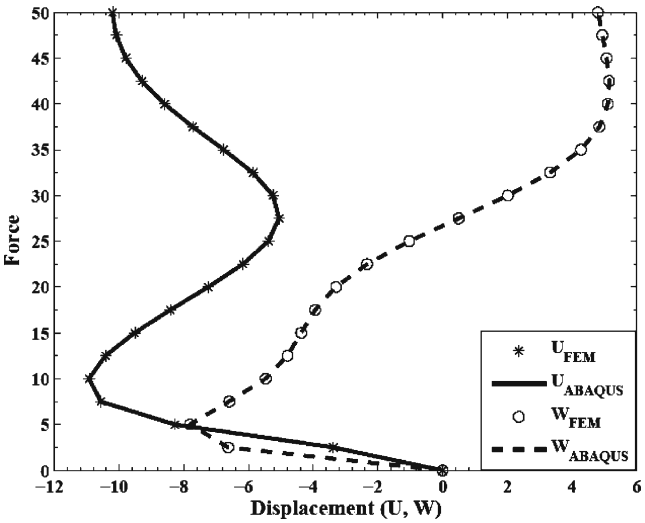

Fig. 4 Comparison of the tip displacements (U for horizontal and W for vertical) obtained with ABAQUS and our finite element codes for the cantilever with a follower tip load

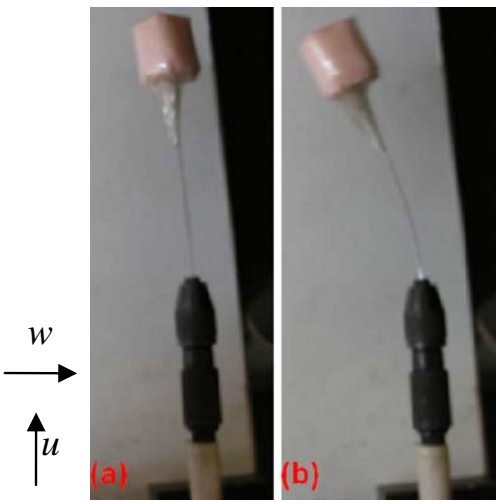

Fig. 6 Undeformed (**a**) and deformed (**b**) configurations of the model of the wheat plant with a grain-bearing spike in a wind tunnel

Table 1 Comparison of the displacements of the cantilever beam subjected to deformation-dependent wind loads obtained experimentally and using the finite element analysis

No.	Velocity (m/s)	FEM solution u (mm), w (mm)	Experimental u (mm), w (mm)	% Error u, w
1	13.35	2.32, 0.06	2.10, 0.05	−9.50, −18.03
2	15.09	2.96, 0.10	2.78, 0.09	−6.08, −6.06
3	18.30	4.25, 0.21	4.02, 0.23	−5.40, 9.76
4	24.24	6.94, 0.55	6.83, 0.58	−1.59, 5.84
5	27.81	8.61, 0.85	8.64, 0.90	0.35, 6.38
6	28.66	9.01, 0.93	9.28, 1.01	2.99, 9.19

3 Optimization problem formulation and solutions

Because uprooting at the ground anchor due to a large reaction moment is the most significant failure mode in wheat plants (Farquhar et al. 2002), we first pose the following problem.

$$\begin{aligned} &\underset{d(x)}{\text{Minimize}} \quad \text{Ground reaction} = M_{\mathrm{R}} \\ &\text{Subject to} \\ &\qquad \text{Equilibrium equation} \\ &\qquad \text{Volume constraint} \\ &\qquad d_{\mathrm{l}} \le d\,(x) \le d_{\mathrm{u}} \end{aligned} \tag{P1}$$

where circular cross-section is assumed with $d(x)$ as the diameter along the length of the beam.[1] But this is an inappropriately posed problem because the stem becomes as flexible as it can be (limited only by the lower bound d_l) in order to deform to achieve $\theta \to \pi/2$ to make the force zero as per (1). Clearly, the stress in that case would exceed the strength and the stiffness is compromised too. The strength consideration can be added in two ways. One method is shown below.

$$\begin{aligned} &\underset{d(x)}{\text{Minimize}} \quad M_{\mathrm{R}} \\ &\text{Subject to} \\ &\qquad \text{Equilibrium equations} \\ &\qquad \max_{x}\,(\sigma\,(x)) \le S \\ &\qquad d_{\mathrm{l}} \le d\,(x) \le d_{\mathrm{u}} \end{aligned} \tag{P2}$$

where σ is the stress and S the permissible strength. The problem was solved using *fmincon* routine in the optimization tool-box of Matlab. The gradients were computed using the finite difference method rather than analytically. Since the number of variables is small, it did not drastically affect the computation time. We note that analytical computation of the gradients is possible but it would be slightly more cumbersome because of the deformation-dependent load. A solution obtained using this formulation is shown in Fig. 7 along with the data used.

Alternatively, the strength criterion can be posed as the primary criterion while trying to lower the reaction moment at the anchor indirectly. This is because the stress is maximum at the ground anchor and is proportional to the reaction moment. This leads us to the formulation shown below.

$$\begin{aligned} &\underset{d(x)}{\text{Minimize}} \quad \left\{S - \max_{x}\,(\sigma\,(x))\right\}^2 \\ &\text{Subject to} \\ &\qquad \text{Equilibrium equations} \\ &\qquad \int_0^L 0.25\pi d^2 dx \le V^* \\ &\qquad \mathrm{d_l} \le d\,(x) \le d_{\mathrm{u}} \end{aligned} \tag{P3}$$

where V^* is the permitted maximum volume, which is taken as one third the volume obtained if the upper bound were reached on the diameter everywhere in the beam. Figure 8 summarizes the results of problem (P3) for different values of S using the same data as was used for problem (P2). It can be noticed in Fig. 8 that as the value of S increases there is a tendency towards compliant designs. In all cases, the reaction moment was less than $F_0 L$ and it gets better (i.e., lower) with increasing values of S. This is in agreement

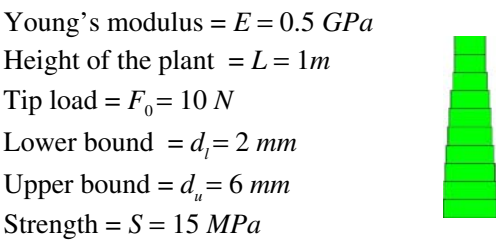

Fig. 7 Data and the optimum diameter profile of the vertical beam (i.e., plant's stem) for problem (P2)

[1] Since the plant, as reported in the literature, selectively changes the material stiffness property, it would be more appropriate to make the Young's modulus as the design variable. But we chose the cross-section here as it is treated as a "size-optimization" problem.

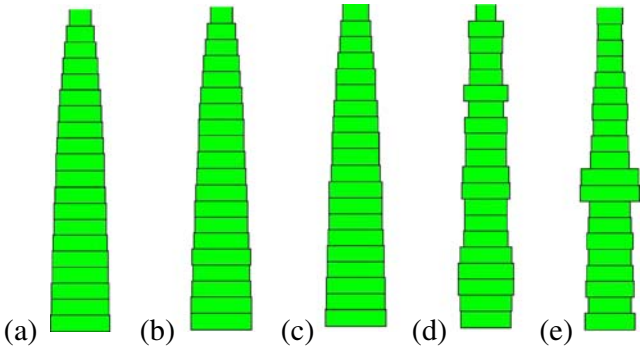

Fig. 8 Optimum cross-sections of problem (P3). **a** $S = 2$ MPa, tip-deflection = 0.0590 m, **b** $S = 3$ MPa, tip-deflection = 0.0591 m, **c** $S = 6$ MPa, tip-deflection = 0.0597 m, **d** $S = 12$ MPa, tip-deflection = 0.0895 m, **e** $S = 15$ MPa, tip-deflection = 0.1146 m. Volume constraint was active only in case (**a**)

with the intuition that higher strength permits larger deflection and larger deflection reduces the tip load and the moment arm about the ground anchor. The area of cross-section profile increasingly tapers upwards and becomes narrower which is an indication of increased flexibility. Similar runs for different values of S can be done for problem (P2) to see that the same results could be observed. It can be noticed that the obtained cross-section profile of Fig. 7 (that had a coarse mesh but the same height as that of Fig. 8a–e) is about the same as those of Fig. 8a–c. But the profiles in Fig. 8d–e are substantially different. Note in particular that the maximum stress is the same in the profiles of Figs. 7 and 8e. This indicates that problems (P2) and (P3) are different and that the formulation influences the obtained cross-section profile. The main difference lies in the fact that in problem (P2) not only the prescribed stress value is met but also the ground reaction moment is minimized. On the other hand, in (P3), only the stress value is met. This difference can be understood by noting that the maximum stress is dependent on the bending moment as well as the moment of inertia (i.e., the cross-section geometry). Hence, the problem (P2) is more appropriate than (P3).

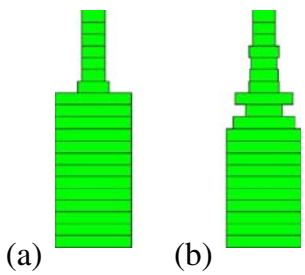

Fig. 9 Optimal cross-section profiles for problem (P4) **a** without the strength constraint using $\Delta/L = 0.2$ **b** with the strength constraint, $S = 15$ MPa and the stiffness constraint, $\Delta/L = 0.2$. $d_l = 3$ mm, $d_u = 10$ mm

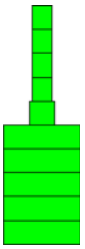

Fig. 10 Optimal cross-section profile for problem (P4) wherein the deformation-dependent load is modeled using (7b) with $S = 15$ MPa, $\Delta/L = 0.3$, $d_l = 2.5$ mm, $d_u = 10$ mm

The horizontal deflection in the last case with $S = 15$ MPa is about 11.5% of the height of the plant, which is high. Furthermore, the solution shown in Fig. 8e had a horizontal deflection of more than 33% of the height of the plant. Thus, it is important to impose an upper bound on the deflection to prevent plants from interfering with their neighbors. This indirectly takes care of the stiffness requirement, which is also important for preventing the mechanical damage to the plant. This is included in the following problem statement.

$$\begin{aligned} &\underset{d(x)}{\text{Minimize}} \quad M_{\mathrm{R}} \\ &\text{Subject to} \\ &\qquad \text{Equilibrium equations} \\ &\qquad \max_{x}\left(\sigma\left(x\right)\right) \le S \\ &\qquad u_{x=L} \le \Delta \\ &\qquad d_{\mathrm{l}} \le d\left(x\right) \le d_{\mathrm{u}} \end{aligned} \tag{P4}$$

Figure 9a–b show the sample results of Problem (P4) without and with strength constraint respectively. It can be seen that the optimum profiles are those that limit the deflection to the upper portion so that it can deform and lower the tip-load as per (1) while retaining stiffness and ensuring that the reaction moment is minimized. It should also be noticed that many elements have reached the upper or lower bounds in both cases. A more accurate modeling of the deformation-dependent load was given in (20b–c). When this is used instead of the approximate load of (1), we obtained the result shown in Fig. 10. In this too, most of the elements reached their upper or lower bounds. These two cases indicate that the optimized profile of the cross-section achieves stiffness (i.e., horizontal tip-load deflection) by effectively decreasing the length of the stem. This is done by pushing the cross-sections of the lower elements to their upper bound.

3.1 Discussion

Given the fact that the load and the moment arm reduce with increasing deflection—which makes the ground reaction small—intuitively we could guess that plants prefer compliant stems. As noted in the introduction, this issue was taken up for an optimization study

because agricultural scientists and genetic engineers have chosen to make the plants grow shorter than their normal height. Engineering view tells us that reduced length implies increased bending stiffness; indeed, if the length is decreased by a factor f, the stiffness increases by a factor of f^3 for transverse bending loads. Stiff stems have more drag (as per (1) and (20b–c)) and large moment arm for the ground reaction moment. Thus, growing them to a reduced height appears to be counter-productive to reducing the ground reaction moment. Thus, it is probably not surprising that the effective elastic modulus decreased in the genetically modified dwarf variety wheat plants. This seems to indicate that the plant found its way to be compliant. This study, through optimization, confirms the intuition that plants do prefer compliant stems when there is no limit on the horizontal tip deflection. This was seen in Fig. 7 where the tip deflection was as much as one third of the stem's height. When the tip deflection is constrained, the optimal stem becomes as flexible as it can be within the limits of that constraint. Another important observation is that the optimal stem profiles are rather straightforward; that is, they taper from the ground to the tip, their significant portion is of uniform cross-section, and many elements reach their lower or upper bounds. This is consistent with the cross-section profiles of the wheat and other cereal crop plants in general.

In this work, as noted in a footnote earlier in the paper, we could have taken Young's modulus as the optimization variable rather than the area of cross-section. This is because the dwarf plants selected changed their modulus. The results of that will be slightly different because the bending stiffness is linearly proportional to the Young's modulus where as the bending stiffness (mainly moment of inertia) is proportional to the fourth power of the diameter. However, the trends in the performance are not likely to be different. By performance, here, we mean that compliant stems are preferred to stiff stems. Thus, the optimization results of the paper support the somewhat counter-intuitive idea that reducing the height of the stem does not reduce the reaction moment to prevent the anchorage rotation. The lack of quantitative comparison between the selectively lowered modulus notwithstanding, the results of this preliminary work suggest that the motivation behind dwarfing of cereal plants should be re-examined from the biomechanics perspective. Further studies should consider buckling under self-weight and resonant frequency and look for quantitative data for comparing with the results of the optimization with. Such data is scarce but exists (Crook and Ennos 1996). The current work, in that sense, is not exhaustive but serves as an example of structural optimization under deformation-dependent load where compliant designs are preferred over stiff designs.

4 Closure

Biomechanical factors are very important for cereal crop plants such as wheat to prevent uprooting due to ground reaction moment, stress, buckling, etc., when they are subject to wind loads. In this paper, we consider only the steady wind loads. As explained in this paper, the determination of the cross-section profile of the plant stem (modeled here as a cantilever beam) leads to a novel structural optimization problem with deformation-dependent loads. An interesting aspect is formulating different optimization problems to see why plants prefer compliant stems as was noticed in the genetically modified dwarf variety (Rht) wheat plants. The results of optimization confirm the counter-intuitive idea that compliant designs are preferred over stiff designs in reducing the ground reaction moment. Competing effects of minimizing reaction moment at the ground anchor, maximum stress and adequate stiffness are considered here. Buckling and dynamic behavior need to be considered in future work along with quantitative comparison with experimental data available in plant biomechanics literature.

Acknowledgements We thank Prof. Raghuraman Govardhan for pointing us to Hoerner's book on fluid dynamic drag and providing the wind tunnel facility for conducting the experiment reported in this paper.

References

Battini JM (2002) Co-rotational beam elements in instability problems. A PhD Thesis technical report from the Royal Institute of Technology, Sweden

Borojevic K (2005) The transfer and history of 'reduced height genes' (*Rht*) in wheat from Japan to Europe. J Heredity 96:455–459

Crisfield MA (1991) Nonlinear finite element analysis of solids and structures, vol 1. Wiley, New York

Crook MJ, Ennos AR (1996) Mechanical difference between free-standing and supported wheat plants, *Triticum aestivum L*. Ann Bot 77:197–202

Farquhar T, Meyer-Phillips H (2001) Relative safety factors against global buckling, anchorage rotation, and tissue rupture in wheat. J. Theor Biol 211:55–65

Farquhar T, Jiang Z, William HW (2002) Competing effects of buckling and anchorage strength on optimal wheat stalk geometry. J Biomech Eng 124:441–449

Farquhar T, Meyer H, Zhou J (2004) Rht dwarfing gene selectively decreases material stiffness of wheat. J Biomechanics (in press)

Hoerner SF (1965) Fluid dynamic drag, fluid dynamics SF Hoerner, Bricktown

Miller AL (2005) Structural dynamics and resonance in plants with nonlinear stiffness. J Theor Biol 234:511–524

Moller H (2002) Analysis and optimization for fluid–structure interaction problems. PhD Thesis, Aalborg University, Denmark

Norman LB (1986) The effects of mechanically-induced stress in plants—a review. Plant Growth Reg 4:103–123

Sivanagendra P (2006) Geometrically nonlinear elastic analysis of frames with application to vision-based force-sensing and mechanics of plant stems. Master of Engineering Project Report, Mechanical Engineering, Indian Institute of Science, Bangalore, India